



Ultrafast optical imaging of the spin Hall effect of light in semiconductors

Jean-Michel Ménard,* Adam E. Mattacchione, and Henry M. van Driel

Department of Physics and Institute for Optical Sciences, University of Toronto, Toronto, Ontario, Canada M5S 1A7

Christine Hautmann and Markus Betz†

Physik-Department E11, Technische Universität München, 85748 Garching, Germany

(Received 26 April 2010; revised manuscript received 21 May 2010; published 6 July 2010)

We experimentally demonstrate a general optical pump-probe technique to observe the spin Hall effect of light (SHEL) in an absorbing medium. In essence, a locally confined pump-induced modification of a material's absorptivity can effectively be used as an induced aperture allowing one to detect the transversely displaced circular polarization components of an incident beam through differential transmission techniques. We consider linear absorption mechanisms such as free-carrier absorption and Pauli blocking as well as nonlinear absorption processes such as two-photon absorption. For absorption mechanisms that do not depend on light polarization, the SHEL of the probe beam is obtained directly, while polarization-dependent properties give an effective SHEL displacement that depends on the action of the SHEL on both pump and probe beams. Using 150 fs pump, 820 nm pump and probe pulses we observe SHEL effects in silicon via free-carrier absorption. SHEL effects are also observed via Pauli blocking at 820 nm and two-photon absorption at 1550 nm in GaAs using ~150 fs pump and probe pulses.

DOI: 10.1103/PhysRevB.82.045303

PACS number(s): 42.65.Re, 42.25.Ja, 42.70.Nq

I. INTRODUCTION

When an optical beam encounters an optical interface at non-normal incidence the right (σ^+) and left (σ^-) circularly polarized beam components experience a displacement transverse to the plane of incidence. This effect was theoretically derived by Fedorov¹ in 1955 in the case of total internal reflection in glass with experimental confirmation given by Imbert² in 1972 for beams of finite cross-section. Hence the effect is historically referred to as the Imbert-Fedorov effect. In the last decade there has been renewed interest in this phenomenon which has been considered theoretically and experimentally for a variety of transparent media and different beam geometries including partial reflection/transmission at an interface.^{3–15} In the case of a linearly polarized beam incident on an optical interface, the transverse separation of σ^+ and σ^- , or spin components, of the light have led some to refer to the Imbert-Fedorov effect as the spin Hall effect of light (SHEL) because of the analogy with the electronic spin Hall effect, wherein an electrical current can produce a transverse separation between carriers of opposite spin.¹⁶ However, the subwavelength (typically nanometer scale) displacements associated with the SHEL have forced experimentalists to use sophisticated schemes to observe it. For example, Imbert used multiple total internal reflections to increase the displacement,² while others have used a multilayered interface,¹⁷ helicoidal eigenstates of a laser cavity,¹⁸ or a position-sensitive detector.¹⁹ Long wavelength (microwave) sources have also been used²⁰ but at the expense of poor beam quality, limiting the resolution. Recently, Hosten and Kwiat, using the language of quantum weak measurements, observed the SHEL in a beam exiting a variable angle prism with a position-sensitive detector⁶ while Qin *et al.* showed the effect for partial reflection.¹²

During the past 50 years all experimental observations of SHEL have involved measurements on a light beam emerg-

ing or reflecting from an air-glass interface. Recently, some of the present authors observed the SHEL at an air-semiconductor interface¹⁵ where absorption was used to resolve the separation between σ^+ and σ^- components. In this recent experiment a tightly focused, linearly polarized, 100 fs pump pulse was shone off-normal incidence onto a thin GaAs sample. In such a configuration, the pulse experiences a transverse separation of its spin components due to the SHEL. The light-polarization dependent selection rules for interband transitions in GaAs dictate that a spatially separated, spin-polarized, electron distribution is imprinted in the material and remains for 10s of picoseconds. This carrier spin population is then temporally and spatially resolved by a probe beam via differential transmission techniques. It was also suggested¹⁵ that other pump-probe techniques, not necessarily involving electron spin effects, could be used to resolve the SHEL in a variety of materials. If true, these results might have implications for a broad range of pump-probe experiments employing tightly focused beams besides providing new ways to image the SHEL.

In this article we demonstrate how general pump-probe techniques can be used to image the SHEL *in situ* in different materials. The basic idea is as follows. A tightly focused pump beam is used to locally alter the transmissivity of an off-normal probe beam. The pump-induced change in the probe beam allows us to consider the pump beam as inducing an effective aperture. As the pump beam is scanned across the spatial profile of the SHEL-split probe beam the transmitted amplitude of the probe beam σ^+ and σ^- components varies, from which one can obtain the SHEL displacement. If the interaction of light beams with the material is independent of light polarization (referred to as the scalar case, below), the SHEL for the probe is observed directly. However, if absorption depends on light polarization (referred to below as the vector case), as it might, e.g., for two-photon absorption (2PA) or circular dichroism of the

type mentioned above,¹⁵ an analysis of the differential transmissivity is sensitive to the SHEL acting on the pump and probe beams.

We experimentally demonstrate this general concept in three different cases, with different materials and different optical absorption mechanisms. In the first experiment, as an illustration of the scalar case, we use pump-induced free-carrier absorption (FCA) in silicon to image the SHEL acting on the probe beam. In the second example we use a technique similar to Ref. 15 to image the SHEL displacement occurring in the pump and the probe beam using Pauli blocking induced by spin populations in GaAs. We provide results on the angular dependence of the SHEL displacement for a wider range of angles than presented in Ref. 15 and also compare the SHEL displacements obtained with *s*- and *p*-polarized incident light. Finally, we apply the imaging technique to sub-band-gap radiation in GaAs and the transverse shifts are resolved using 2PA of simultaneously impinging pump and probe pulses. All experimental results are shown to be in good agreement with the theoretical expectations for the SHEL.

The remainder of this paper is organized as followed. In Sec. II, we review some of the theoretical foundations of the SHEL and introduce the formalism to compare that theory to the measurements we obtained via scalar and vector interactions between light and matter. The generalized aperture method to image the SHEL is also presented in that section, and the experimental details related to the three different imaging techniques used in this paper are given in Sec. III. Finally, we present and discuss in Sec. IV the results of the SHEL displacements.

II. THEORY

A. SHEL displacement

The transverse shift of a spatially confined light beam crossing from air into a medium of real refractive index, n , has been discussed and calculated in the literature using different approaches. Perhaps the most physically satisfying approach uses the fundamental law of conservation of angular momentum.^{3–5,21,22} According to Noether's theorem, the total (spin and orbital) angular momentum must be conserved along the axis of symmetry of the system which is, for an off-normal incident beam at a planar optical interface, perpendicular to the interface plane. To conserve total angular momentum, the center of the reflected and transmitted components of an incident circularly polarized beam shift in the plane of the interface along a transverse direction perpendicular to the plane of incidence. A more typical method to determine the SHEL displacements consists in decomposing the incident, reflected, and transmitted beams of finite cross section into their plane wave constituents and applying the Fresnel relations to the *s* and *p* components of the individual plane waves. The spatial dependence of the reflected and transmitted beams is retrieved by summing over all partial plane waves which can be done analytically using the paraxial approximation.^{4–6,23–26}

The total SHEL displacement, d , between the σ^+ and σ^- components of a linearly polarized beam varies with the

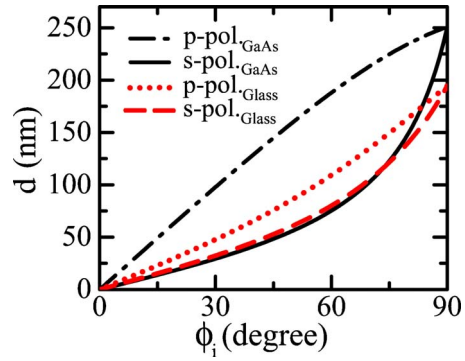


FIG. 1. (Color online) Calculated SHEL displacement [Eq. (1)] as a function of the angle of incidence ϕ_i and the polarization of a light beam ($\lambda=820$ nm) impinging on glass or a semiconductor such as GaAs or Si.

wavelength of the light, its polarization state and the angle of incidence of the beam at the interface, ϕ_i . For *p*- or *s*-polarized beams propagating in air and impinging on a nonabsorbing medium, the SHEL displacement (d^p and d^s , respectively) is found to be^{4,6}

$$d^p(\phi_i) = (\lambda/\pi)[\cos(\phi_r) - t_s/t_p \cos(\phi_i)]/\sin(\phi_i),$$

$$d^s(\phi_i) = (\lambda/\pi)[\cos(\phi_r) - t_p/t_s \cos(\phi_i)]/\sin(\phi_i). \quad (1)$$

Here ϕ_r is the angle of refraction and $t_{s,p}$ are the transmission Fresnel coefficients for *s*- and *p*-polarized light. In the case of weakly absorbing materials (imaginary part of complex refractive index $\ll n$), such as the semiconductors considered in our experiments, Eq. (1) remains valid. If the real and imaginary parts of the material refractive index are comparable, one can obtain d by using the complex refractive index in Eq. (1) and taking the real part of the right hand side. The imaginary part of the refractive index can be associated with an angular shift between the σ^+ and σ^- components.²⁷ Figure 1 shows theoretical values for the transmitted (but internal to the medium) beam for $n=1.5$ (glass) and $n=3.6$ (close to the value for Si and GaAs in our experimental conditions). Note that the maximum separation between the σ^+ and σ^- components (at $\phi_i=90^\circ$) mainly depends on the wavelength, and only marginally on the refractive index (if n is large): $d^{(p,s)}(\phi_i=90^\circ) = (\lambda/\pi)\sqrt{1-1/n^2}$.

B. Generalized aperture method to measure SHEL

We outline the theoretical basis from which to determine the SHEL displacement in a material using pump-probe interactions with the pump beam effectively inducing an aperture, altering the transmission characteristics of the probe beam. We consider the two cases corresponding to whether the interaction of light with matter is independent of polarization (scalar case) or dependent on light polarization (vector case).

1. Scalar interaction between light and matter

Referring to Fig. 2(a), the sample front surface is taken to coincide with the *x*-*y* plane with the *z* axis normal to the

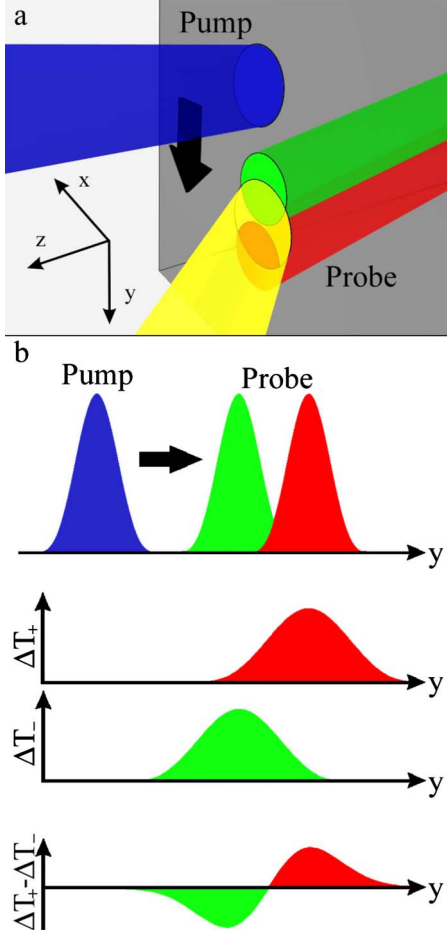


FIG. 2. (Color online) (a) Normal incident pump beam scanned across the circular components of the probe beam which are spatially separated at the interface because of the SHEL. (b) Transmission change and differential transmission signals for a general case.

interface. We consider *p*- or *s*-polarized beams only, with the *x*-*z* plane defining the plane of incidence. The SHEL displacement between the σ^+ and σ^- components of a beam is therefore along the *y* axis. The beams are assumed to have a Gaussian spatial profile; other spatial profiles could also be considered, but this will not substantively change the arguments below, only some numerical factors. Note that, regardless of the angle of incidence, the *y* dependence of the electric field of the beam behind the entrance surface is always of the form $G_{w_{e,r}}(y) \propto \exp(-y^2/w_{e,r}^2)$ where $w_{e,r}$ is a characteristic beam width for the pump/excitation (*e*) or probe pulse (*r*) just behind the entrance surface.

With a tightly focused probe beam centered at $(x,y)=(0,0)$ on the sample surface, a tightly focused pump beam, centered at $(0,y_e)$ is scanned along the *y* direction (y_e varies). The pump beam induces a change in the transmission of the σ^+ and σ^- components of the probe beam, $\Delta T_{\pm} = T_{\pm} - T_{\pm}^{(0)}$, where T_{\pm} and $T_{\pm}^{(0)}$ are the transmission of the probe with and without the pump beam, respectively. We assume that $\Delta T_{\pm}/T_{\pm}$ does not depend on the polarization of pump or probe beam as would occur via a scalar interaction, e.g., through an absorption coefficient that depends on a scalar linear susceptibility, carrier density, carrier or lattice tem-

perature, etc. In the absence of SHEL effects, ΔT_{\pm} depends on the spatial convolution of pump and probe beams with $\Delta T_{\pm}(y_e) \propto \exp(-y_e^2/w^2) = G_w(y_e)$ where $w = \sqrt{w_e^2 + w_r^2}/2$. If the probe beam experiences a SHEL separation of d_r between its σ^+ and σ^- components then $\Delta T_{\pm}(y_e) \propto G_w(y_e \pm d_r/2)$. When $w \gg d_r$ (essentially always the case since $w > \lambda$), $\Delta T_+ - \Delta T_- \propto G_w(y_e + d_r/2) - G_w(y_e - d_r/2) = d_r [\partial G_w(y_e)/\partial y_e]$, indicative of an effective circular dichroism. Hence, although ΔT_+ and ΔT_- are approximately of the same value, their difference is proportional to d_r . Indeed if we define

$$w \sqrt{\frac{e}{2} \frac{|\Delta T_- - \Delta T_+|_{y_e=w/\sqrt{2}}}{|\Delta T_+|_{y_e=0}}} = \tilde{d} \quad (2)$$

where $y_e = w/\sqrt{2}$ corresponds to the maximum of $\partial G_w(y_e)/\partial y_e$ and $y_e = 0$ corresponds to the maximum of $G_w(y_e)$, then it is straightforward to show that for this scalar interaction

$$\tilde{d} = d_r^{(p,s)}. \quad (3)$$

This result is independent of whether the pump beam experiences a SHEL effect.

An example of a pump-probe interaction that does not depend on beam polarization is *free-carrier absorption*. In a semiconductor, electrons and holes (e.g., optically excited by a pump beam) can themselves absorb radiation with the assistance of other particles to satisfy momentum conservation. If the probe beam energy is less than the fundamental energy gap and the delay time between pump and probe pulses, τ , is larger than pump and probe pulse durations, free-carrier absorption (including possible intervalence and interconduction band absorption) is the dominant absorption mechanism. The change in transmission experienced by σ^{\pm} probe components is independent of polarization and only depends on the number of carriers, N , excited by the pump beam. Indeed one can write

$$\Delta T_{\pm} \propto -\sigma_{(FCA)} N, \quad (4)$$

where $\sigma_{(FCA)}$ is the total free-carrier absorption cross section for electrons and holes. Hence, for free-carrier absorption of the probe beam induced by the pump beam, $\tilde{d} = d_r^{(p,s)}$.

2. Vector/polarization interaction between light and matter

If the interaction of pump or probe beam with the material depends on light polarization the simple picture used above leading to $\tilde{d} = d_r^{(p,s)}$ is not complete. Such interactions include spin-dependent Pauli blocking, two-photon absorption, and the optical Kerr effect in an optically anisotropic medium. As seen below the SHEL acting on a non-normally incident pump beam can also induce circular birefringence in the probe beam, resulting in an additional contribution to the differential transmission signal. Overall, we find that the differential transmission expression of Eq. (2) leads to

$$\tilde{d} = \eta d_r^{(p,s)} - \rho d_e^{(p,s)}, \quad (5)$$

where $d_e^{(p,s)}$ is the SHEL separation between the σ^+ and σ^- components of the *p*- or *s*-polarized pump beam and ρ and η

are coefficients that depend on the polarization dependent beam interaction. We now consider two such interactions, Pauli blocking and two-photon absorption/optical Kerr effect.

(i) *Pauli blocking in GaAs.* The optical excitation of a zincblende semiconductor such as GaAs with circularly polarized pump photons whose energy, $\hbar\omega$, is greater than the fundamental gap but less than the spin-orbit split-off gap, creates spin-polarized electrons (holes) in the conduction (valence) band.²⁸ While hole spin polarization relaxes in ~ 100 fs,²⁹ electron spin polarization remains for a time that is the lesser of the spin depolarization time and the electron-hole recombination time. Typically these times are >10 ps.²⁸ Based on selection rules a σ^+ polarized pump beam generates a density of \downarrow electrons, N_\downarrow , that is (maximally three times) greater than the density of \uparrow electrons, N_\uparrow , and vice versa for σ^- light. The quantity $P=(N_\downarrow-N_\uparrow)/(N_\downarrow+N_\uparrow)$ defines a degree of spin polarization that tends to zero with increasing time after the carrier injection. The initial value of spin polarization, P_i , depends on the exact optical absorption selection rules for a given photon energy and has a maximum value of $P_i=0.5$ in GaAs (occurring for exact band edge excitation).

A subpicosecond circularly polarized probe pulse delayed from the pump pulse by less than the spin polarization relaxation time, experiences a reduced absorption that depends on the spin occupancy of optically coupled states in the conduction and the valence band. Because the valence band density of states is much larger than that of the conduction band, once excited carriers thermalize, the difference in optically coupled states is much less than that of the conduction band. Therefore, the change in transmission of the σ^+ and σ^- components of the probe beam is dominated by electron spin density. Due to differential Pauli blocking effects resulting from the electron spin populations the σ^\pm probe transmission takes the form,^{30,31}

$$\Delta T_\pm \propto \frac{1 \pm P_i}{2} N_\downarrow + \frac{1 \mp P_i}{2} N_\uparrow. \quad (6)$$

With a differential transmission which includes the effect of the SHEL displaced opposite electron spin populations injected by the σ^\pm components of a pump beam one can again calculate \tilde{d} . The details are given in Appendix A. The Pauli blocking (PB) mechanism leads to

$$\tilde{d} = d_r^{(p,s)} - \rho_{(PB)} d_e^{(p,s)}, \quad (7)$$

where the factor $\rho_{(PB)}$ has a maximum value of $P_i^2=0.25$. Note that once the spin polarization vanishes, one again has $\tilde{d}=d_r^{(p,s)}$ as expected.

(ii) *Two-photon absorption/optical Kerr effect.* A nonlinear optical interaction involving the simultaneous presence of pump and probe photons can also be used to alter the transmission of the probe beam. Two-photon absorption (2PA) and the optical Kerr effect (OKE) differ from the two previously described pump-probe interactions in that they require time overlap between the pump and the probe pulses. We consider here that the probe beam is very weak compared to the pump beam and that the photon energy is less than the

fundamental band gap of the semiconductor. We thereby neglect, *inter alia*, free-carrier absorption of probe photons by carriers generated by 2PA of the pump beam. For degenerate pump and probe beams with frequency ω 2PA and OKE are governed by a complex valued fourth rank tensor $\chi_{ijkl}^{(3)}(-\omega; -\omega, \omega, \omega) = \chi'_{ijkl} + i\chi''_{ijkl}$. We consider an *excitation* (pump) field, $\vec{E}_e = E_e \hat{e}$ and a probe field $\vec{E}_r = E_r \hat{r}$ with unit polarization vectors, \hat{e} and \hat{r} . For zincblende materials like GaAs, there are only three independent tensor elements of this $\vec{\chi}^{(3)}$ *viz.*, χ_{xxxx} , χ_{xxyy} , and χ_{xyxy} . Appendix B gives the details of how the \tilde{d} derived from 2PA and OKE effects depends on d_r and d_e in the case of copolarized *s*- or *p*-polarized pump and probe beams incident on a (001)-oriented surface of GaAs with the plane of incidence containing the [110]-, [1̄1̄0]-, [100]- or [010]-crystal axis. We find that

$$\tilde{d}_{(2PA)} = \eta_{(2PA)} d_r^{(p,s)} - \rho_{(2PA)} d_e^{(p,s)}. \quad (8)$$

When the [110]- or [1̄1̄0]-crystal axis is contained within the plane of incidence, the coefficients $\eta_{(2PA)}$ and $\rho_{(2PA)}$ are given by

$$\begin{aligned} \eta_{(2PA)} &= \frac{(\chi''_{xxxx} + \chi''_{xyxy})}{(\chi''_{xxxx} + \chi''_{xxyy} + 2\chi''_{xyxy})}, \\ \rho_{(2PA)} &= \frac{(\chi''_{xxyy} - \chi''_{xyxy})}{(\chi''_{xxxx} + \chi''_{xxyy} + 2\chi''_{xyxy})}. \end{aligned} \quad (9)$$

However, if the [100]- or [010]-crystal axis is the one contained within the plane of incidence, we have

$$\begin{aligned} \eta_{(2PA)} &= \frac{(\chi''_{xxxx} + \chi''_{xyxy})}{2(\chi''_{xxxx})}, \\ \rho_{(2PA)} &= \frac{(\chi''_{xyxy} - \chi''_{xxyy})}{2(\chi''_{xxxx})}. \end{aligned} \quad (10)$$

Note that in this regime of weak nonlinearity, the real part of the nonlinear susceptibility does not appear within the coefficients $\eta_{(2PA)}$ and $\rho_{(2PA)}$. However, when one of the [100], [010], [110], or [1̄1̄0] axis of the GaAs sample is not aligned in the plane of incidence, the real part of $\chi^{(3)}$ generates a pump-induced circular birefringence in the probe beam which is independent of the SHEL. Such circular birefringence appears as a Gaussian offset in the differential signal of Eq. (2) and therefore prevents one from obtaining the SHEL displacement using Eq. (8).

III. EXPERIMENT

The mechanisms used to experimentally observe SHEL as part of the general manifestation of pump-probe experiments are free-carrier absorption, Pauli blocking effects and two-photon absorption. The former two can be carried out with a pump-probe delay τ which is long compared to the temporal width of the beams and short compared to the spin relaxation time of the pump-induced carriers. On the other hand the 2PA experiments must be carried out under $\tau=0$ conditions.

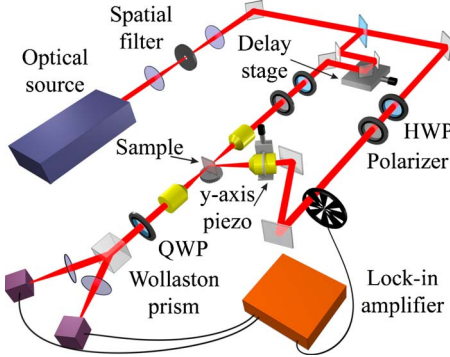


FIG. 3. (Color online) Pump-probe experimental configuration used to observe the SHEL.

To demonstrate these mechanisms we have used Si and GaAs as well as two different ultrafast laser sources. The first optical source is a homebuilt Ti:sapphire laser delivering 150 fs pulses at a repetition rate of 76 MHz and a photon energy of 1.50 eV ($\lambda=820$ nm). The second laser is an amplified Toptica FFS Er:fiber laser producing 120 fs pulses at a repetition rate of 80 MHz with a central photon energy of 0.80 eV ($\lambda=1550$ nm). While photons of 1.50 eV energy resonantly excite free carriers in Si (indirect band gap 1.1 eV at 295 K) and GaAs (direct band gap 1.42 eV at 295 K), a photon energy of 0.80 eV is well suited to induce 2PA in GaAs. The general experimental setup used for all experiments is represented in Fig. 3. Pump and probe pulse trains are tightly focused with two aspheric lenses and have comparable diameter (the probe is typically 15% smaller) at the sample. The incident beam propagation directions are separated by a fixed angle $\psi \sim 55^\circ$ which is limited by the size of the optical components. We rotate the sample (Fig. 4) to investigate the dependence of the angle of incidence of the probe ϕ_i on \tilde{d} . Including this angular separation in Eq. (5), we obtain

$$\tilde{d}(\phi_i) = \eta d_r(\phi_i) - \rho d_e(\phi_i - \psi), \quad (11)$$

which yields a positive offset proportional to d_e at $\phi_i=0$.

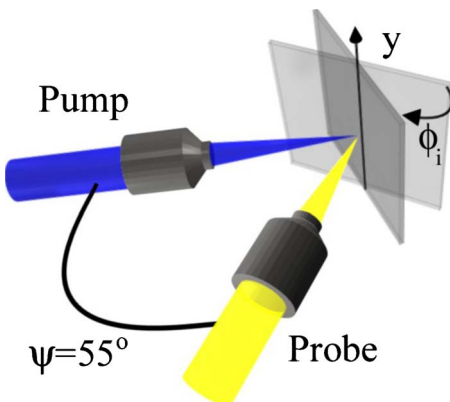


FIG. 4. (Color online) Pump and probe beams are tightly focused onto a sample which is rotated to investigate the SHEL as a function of the angle of incidence of the probe beam ϕ_i .

A piezotransducer is used to scan the pump excitation spot across the probe beam. The probe light is collected with a large aperture lens and then passed through a quarter wave plate and a Wollaston prism. Two photodiodes and a lock-in amplifier referenced to the chopped excitation pulse allow to resolve the change in transmission of the circular components (σ^+ and σ^-) of the probe beam and consequently resolve any circular dichroism induced by the pump pulse.

A. Free-carrier absorption in Si

In a first set of experiments, we use the $\lambda=820$ nm Ti:sapphire to observe the SHEL in a 10 μm thick nominally undoped (100)-oriented Si wafer ($n \sim 3.7$ at $\lambda=820$ nm). A 5 mW pump beam is used to generate an estimated free-carrier density of $\sim 1 \times 10^{17} \text{ cm}^{-3}$, and a *p*-polarized probe beam has an average power of ~ 3 mW. The polarization of the pump beam for this experiment can be arbitrarily chosen in order to reduce noise from scattered light since the free-carrier absorption mechanism in Si does not allow the SHEL acting on the pump beam to be detected. In other words, the small separation between the free-carrier populations generated by opposite circular components of the pump beam remains indistinguishable by the probe beam in our experiment. We measure a maximum decrease in transmission of 0.1% of the probe beam on a single detector due to pump-induced free-carrier absorption and the full width at half maximum (FWHM) of this signal corresponding to the spatial convolution of the pump and probe pulses is $4.5 \pm 0.5 \mu\text{m}$. This FWHM approaches the diffraction limit for our experimental conditions and can vary slightly depending on the quality of the alignment.

The weak signals obtained with Si requires additional experimental steps to extract a background-free differential signal associated with the SHEL displacement. First, a reference scan at a time with delay of $\tau \sim 2$ ps preceding the pump pulse is taken for each data point to subtract background effects associated with the accumulation and the diffusion of the carriers due to the long carrier lifetime in Si ($> 1 \mu\text{s}$).³² Also, we noticed a pump-induced lensing effect which scales linearly with the pump power and, as a result, cannot be eradicated by lowering the pump power. This effect resulted in a slight pump-induced tilt of the probe beam which could be minimized by adjusting the optical components following the sample. Finally, for every data point at a fixed ϕ_i , we took two sets of measurements using orthogonal orientations of the quarter wave plate located after the collection lens. Since the two differential signals obtained with this technique must have opposite signs, we can then subtract any offset attributed to lensing effects. Note that the later technique to minimize parasitic signals was only necessary for the FCA experiments because the transmission changes induced by thermal effects were then comparable in magnitude to the FCA signal.

B. Pauli blocking in GaAs

A 500 nm thick (001)-oriented GaAs sample ($n \sim 3.6$ at $\lambda=820$ nm) mounted on a glass substrate is also used with resonant optical excitation from the Ti:sapphire laser to re-

solve the SHEL. The pump beam has an average power of ~ 2.5 mW generating an estimated peak carrier density of $\sim 3 \times 10^{18}$ cm $^{-3}$ while the probe pulse has an average power $\ll 1$ mW. Probe pulses are delayed by ~ 2 ps relative to the pump pulses, a time longer than the carrier cooling time³³ of ~ 500 fs but less than the electron spin relaxation time of >10 ps in GaAs (Ref. 28); any hole spin orientation in GaAs is expected to have completely decayed in <1 ps.²⁹ We investigate the influence of the polarization state on the SHEL displacement using in turn the *p* and *s* polarization in the probe beam which can be selected using a half wave plate and a polarizer positioned in front of the focusing optics. The pump is kept *p*-polarized since an *s*-polarized pump beam generates additional scattered light due to higher reflection at the interface thus decreasing the signal to noise ratio. Moreover, the change in the signals obtained by varying the orientation of the linear polarization of the pump beam is expected to be comparable to the resolution limit of our experiment. The typical FWHM of ΔT_{\pm} is 4.7 ± 0.5 μm and the peak normalized signal corresponds to a 10% increase in transmission caused by Pauli blocking. Finally, in a separate experiment, we determined $\rho_{(PB)} \sim 0.18$ using a circularly polarized pump beam as shown in Eq. (A5). Note that the contribution from pump-probe walk off effects and projection of the spins onto the direction of the probe beam are negligible but nonetheless included indirectly in the measurement of the coefficient $\rho_{(PB)}$. Note also that the partial reflection of the pump beam from the back surface of the sample also generates a SHEL displacement in the pump beam of a magnitude similar to the SHEL displacement associated with the beam transmission through the sample's front surface. However, in our experimental configuration, a combination of factors prevent us from detecting this additional contribution: the fraction of the reflected pump power at the GaAs-glass interface is $<25\%$, the SHEL acting on the pump beam is a relatively weak contribution to the measured signal ($\rho_{PB} < \eta_{PB}$) and the linear optical absorption in GaAs attenuates the power of the pump beam by $\sim 50\%$ before back surface reflection.

C. 2PA in GaAs

For the observation of the SHEL via 2PA in a GaAs wafer, we use an amplified Er:fiber optical source with photon energy well below the band gap of GaAs. The (001)-oriented GaAs sample is 500 μm thick, although the interaction length inside the semiconductor is only ~ 30 μm due to the angular separation of the pump and the probe beams and the tight focusing optics. Because of this relatively short interaction length, we can also neglect the contribution of the SHEL displacement in the pump beam due to its partial reflection at the sample back surface. The pump and probe beams are collinearly polarized and have an average power of ~ 10 and ~ 2.5 mW, respectively. Furthermore, their Gaussian spatial convolutions have a FWHM of $\sim 10 \pm 1$ μm , which is also close to the diffraction limit for the wavelength used. Overlapping both pump and probe pulses in time and in space generates a typical decrease in transmission of the probe of 2% due to 2PA.

For this experiment, the GaAs sample is rotated about the surface normal to reduce the amount of pump-induced circular birefringence acting on the probe beam. Such nonlinear birefringence generates an imbalanced signal on the detectors and consequently cancels the benefits of the background free technique we use to detect any circular dichroism ($\Delta T_+ - \Delta T_-$). In order to minimize the pump-induced birefringence on the probe beam and maximize the 2PA signal in the experiment, the principal [100] axis of the sample is oriented 45° relative to the plane of incidence. The *p*- or *s*-polarized pump and probe are therefore aligned along the [110]- or [1̄10]-crystal axis.

In a separate experiment we also determined the value of the coefficients $\eta_{(2PA)}$ and $\rho_{(2PA)}$ of Eq. (8). Using the concept of effective susceptibility defined in Eq. (B7), we can express Eq. (9) as

$$\begin{aligned} \eta_{(2PA)} &= \frac{\chi''_{\text{eff}}(\sigma^{\pm}; \hat{\ell}, \hat{\ell}, \sigma^{\pm})}{\chi''_{\text{eff}}(\hat{\ell}; \hat{\ell}, \hat{\ell}, \hat{\ell})}, \\ \rho_{(2PA)} &= \frac{\chi''_{\text{eff}}(\sigma^{\pm}; (\sigma^{\pm})^*, \sigma^{\pm}, \sigma^{\pm}) - \chi''_{\text{eff}}(\sigma^{\mp}; (\sigma^{\pm})^*, \sigma^{\pm}, \sigma^{\mp})}{2\chi''_{\text{eff}}(\hat{\ell}; \hat{\ell}, \hat{\ell}, \hat{\ell})} \end{aligned} \quad (12)$$

where $\hat{\ell}$ is the linear polarization state of both incident pump and probe beams used in the SHEL experiment. Note that Eq. (12) is also valid if both beams are oriented along the [100]- or [010]-crystal axis. Since the total pump-probe 2PA coefficient (β) is proportional to the effective susceptibility for given polarization states of the interacting beams ($\beta \propto \chi''_{\text{eff}}$), we can determine experimentally the values of $\eta_{(2PA)}$ and $\rho_{(2PA)}$ by measuring β corresponding to each χ''_{eff} of Eq. (12). Using a separate experimental setup with the appropriate polarization optics to compare these normalized pump-induced transmission changes in the probe beam, we obtain $\eta_{(2PA)} = 0.67 \pm 0.02$ and $\rho_{(2PA)} = 0.10 \pm 0.01$. Including these experimental values and the angle dependence in Eq. (8) we obtain

$$\tilde{d}(\phi_i) = (0.67)d_r^{(p,s)}(\phi_i) - (0.1)d_e^{(p,s)}(\phi_i - \psi). \quad (13)$$

IV. RESULTS

A. Free-carrier absorption

The SHEL displacement at an air-Si interface is considered for pump-probe interactions through free-carrier absorption as described in Sec. III A. Figure 5 shows the change in transmission and circular dichroism revealing a separation $d = 130 \pm 20$ nm between the circular components of the probe beam. This particular experiment uses a *p*-polarized probe at $\phi_i = 32^\circ$.

We rotate the sample as shown in Fig. 4 and obtain a set of data similar to Fig. 5 for various ϕ_i . From the measured ΔT_{\pm} and $\Delta T_+ - \Delta T_-$, d can be extracted and Fig. 6 shows its ϕ_i dependence. The data are in good agreement with the theory derived exclusively from Eq. (1). Note that the data

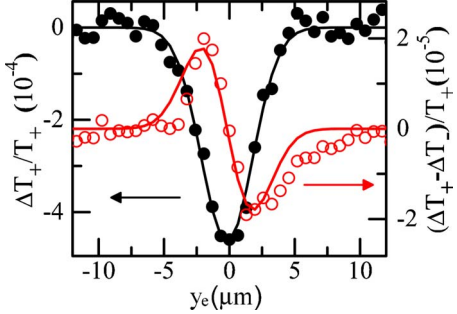


FIG. 5. (Color online) Change in transmission of a circular component of a p -polarized probe beam at $\phi_i=32^\circ$ focused onto a 10 μm thick Si sample (closed circles). The open circles show the circular dichroism proportional to the SHEL displacement in the probe beam.

point at $\phi_i=-20^\circ$ shows a negative displacement, as we expect for negative angles, but differs notably from the theoretical predictions. As discussed in Sec. III A, weaker signals in Si make our technique more vulnerable to various artifacts. Although we succeeded in identifying the main sources of errors and circumvent them via additional experimental precautions described previously, we attribute the deviation of the data point at $\phi_i=-20^\circ$ from theoretical predictions to an additional offset due to enhanced thermal lensing.

B. Pauli blocking in GaAs

Figure 7 shows typical transmission change obtained with resonant excitation in GaAs for the experimental conditions described in Sec. III B. This particular experiment uses a p -polarized probe at $\phi_i=43^\circ$, closely resembling the configuration depicted in Fig. 2(a). Note that the change in transmission (ΔT_\pm) is positive. As explained in the theory section (Sec. II B), the spin-dependent interaction provides an opportunity to detect simultaneously the SHEL displacements induced in the pump and the probe beam. Using Eq. (2) we extract from Fig. 7 a displacement $\tilde{d} \sim 140 \pm 13$ nm which is mainly related to the separation of the circular components of the probe beam since the pump beam is almost at normal incidence ($\phi_i-\psi=-12^\circ$).

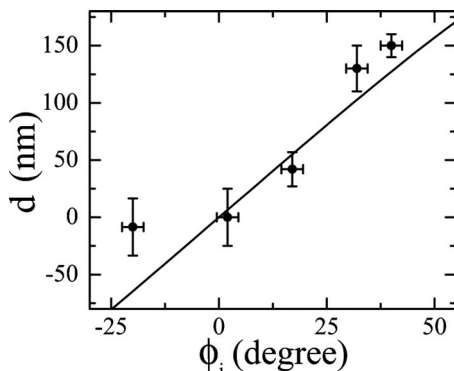


FIG. 6. SHEL displacement in a p -polarized probe beam at an air-Si interface as a function of ϕ_i . The solid line represents a theoretical prediction based on Eq. (1).

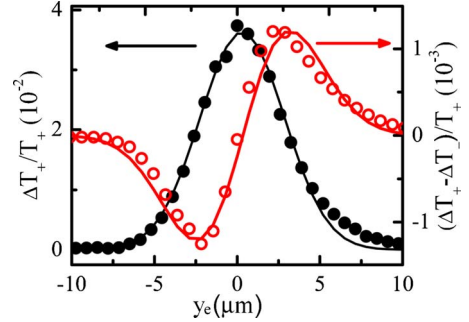


FIG. 7. (Color online) Change in transmission of a circular component of a p -polarized probe beam (closed circles) as a function of the scanning position of the pump beam (y_e) in a 500 nm thick GaAs sample for $\phi_i=43^\circ$. The open circles show the difference between the change in transmission obtained for both circular components.

The angular dependence of the measured separation \tilde{d} between the circular components of the probe transmitted in GaAs (Fig. 8) is in good agreement with the theory [Eq. (7)] taking into account the two contributions from the SHEL induced displacement in the pump and probe beam. To clearly illustrate the angular dependence of the two separate contributions, we included in the inset of Fig. 8 the expected displacements (d_r and $\rho_{(PB)}d_e$) calculated from Eq. (1) and considering our experimental configuration. The SHEL acting on the probe beam, which is the dominant contribution, is approximately linearly proportional to ϕ_i while the weaker contribution from the displacement related to the SHEL acting on the pump beam is roughly linearly proportional to $(\psi-\phi_i)$.

C. 2PA in GaAs

For the 2PA mechanism the change in transmission ΔT_\pm obtained in these experiments has the same sign as the measurements presented in Fig. 5 since 2PA also decreases the transmission of the probe beam. Figure 9 shows \tilde{d} as a function of ϕ_i using either collinearly p - (blue squares) or s -polarized (red dots) pump and probe beams. Note that the larger optical wavelength of the source ($\lambda=1550$ nm) entails correspondingly larger measured displacements in comparison to the results presented in the two previously described experiments at $\lambda=820$ nm. The data in Fig. 9 are compared to the theoretical SHEL separations of the probe's circular components at the air-GaAs interface derived from Eq. (1) (dashed lines) and shows a fair agreement. However, as mentioned in Sec. II B 2, a more complete theory taking into account the polarization dependence of 2PA is required to estimate \tilde{d} at a given angle ϕ_i . This theoretical curve corresponding to the vector case is given by Eq. (13) (solid lines in Fig. 9) where the coefficients scaling the different contributions from d_e and d_r to the measured displacement are determined experimentally as described in Sec. III C. We notice better agreement between the data and the solid lines corresponding to the vector interaction case than the dashed lines corresponding to a scalar interaction between light and matter.

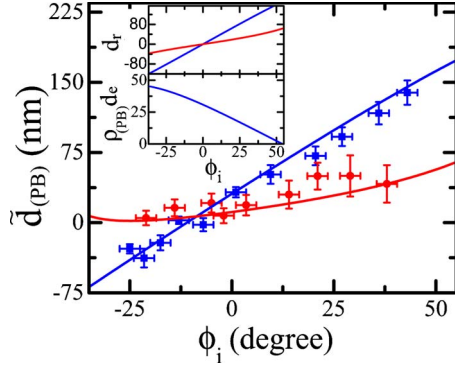


FIG. 8. (Color online) Measured displacement induced by the SHEL acting on a *p*- (blue squares) or *s*-polarized (red dots) probe beams and a *p*-polarized pump beam incident on a thin GaAs sample. The angle between the pump and the probe is kept fixed at $\psi=55^\circ$ as we rotate the sample and vary the angle of incidence of the probe (ϕ_i) on the sample. The lines are based on theoretical predictions in Eq. (1) and (7). The inset shows the separate theoretical contributions from the probe and the pump (in nm).

V. CONCLUSION

In summary, we have resolved the subwavelength displacements induced by the SHEL at an air-Si and air-GaAs interface. Our experimental technique relies on the pump-induced polarization change of a probe beam impinging on a material at off-normal incidence. We present measurements of the SHEL displacement and theoretical predictions for scalar interactions (FCA) and vector interactions (Pauli blocking and 2PA) between the light and matter. The SHEL separation has been investigated as a function of the angle of incidence, the polarization state and the wavelength of the light, and the results confirm the theory.

Finally, the results presented in this paper could be of some interest to any experimentalist conducting precision measurements based on the polarization state of a beam transmitted through a nonlinear material. For instance, Raman induced Kerr effect spectroscopy (RIKES) and other nonlinear spectroscopy techniques rely on an experimental configuration similar to the one presented in this paper. It is already known⁶ that a linearly polarized beam does not retain the same polarization after its transmission through a wedge of isotropic material. However, we here demonstrated that a measurable circular dichroism can also be induced on a linearly polarized beam transmitted through a slab of isotropic material (with parallel optical interfaces) if this beam is impinging off-normal incidence and interacts with another light beam producing an induced aperture in the material.

ACKNOWLEDGMENTS

We acknowledge useful discussions with J. E. Sipe and A. L. Smirl and Natural Sciences and Engineering Research Council of Canada (NSERC) for financial support. M. Betz appreciates support from the Alexander von Humboldt Foundation.

APPENDIX A: CALCULATIONS OF \tilde{d} OBTAINED VIA SPIN-DEPENDENT PAULI BLOCKING

For a zincblende semiconductor such as GaAs, as indicated in Sec. II B 2 the SHEL acting on a *p*- or *s*-polarized

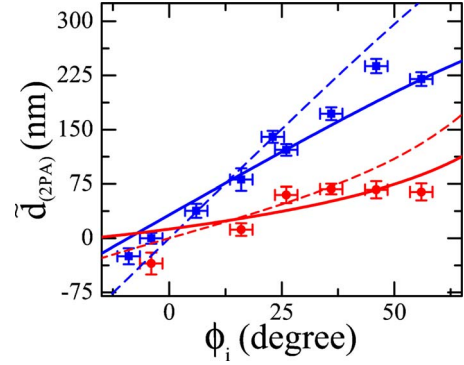


FIG. 9. (Color online) Measurements of \tilde{d} in a 500 μm thick GaAs sample using *s*- or *p*-copolarized pump and probe beams and 2PA as the imaging mechanism. The dash lines represent a theoretical prediction of the total SHEL displacement based on Eq. (1) while the solid lines are the modified theoretical prediction taking into account the correction for the polarization anisotropy of the 2PA coefficient.

pump beam results in the injection of two spatially displaced electron spin populations, separated by $d_e^{(p,s)}$. Here we derive the relationship between \tilde{d} and d_r and d_e when a *p*- or *s*-polarized probe beam is used. If the SHEL acts on both the pump and probe beam, with the notation of Sec. II B, their respective field inside the material is of the form

$$\vec{E}_{e(r)} = \frac{E_{e(r)}}{\sqrt{2}} [G_{w_{e(r)}}(\tilde{y}_{e(r)} + d_{e(r)}/2)\sigma^+ + G_{w_{e(r)}}(\tilde{y}_{e(r)} - d_{e(r)}/2)\sigma^-] \\ = (\mathcal{E}_+)_{e(r)}\sigma^+ + (\mathcal{E}_-)_{e(r)}\sigma^-, \quad (\text{A1})$$

where $\tilde{y}_r = y$ and $\tilde{y}_e = y - y_e$ to allow the pump and the probe beam to be centered at different positions along the *y* direction. Note that the beams also have a Gaussian spatial dependence along the *x* direction, however we suppress this since it does not influence the final result. From Eq. (A1) and the injected degree of spin polarization by a circularly polarized beam defined in Sec. II B 2, the density of spin \uparrow and \downarrow carriers (N_\uparrow and N_\downarrow) in the semiconductor is

$$N_\downarrow \propto \frac{1+P}{2}(I_+)_e + \frac{1-P}{2}(I_-)_e,$$

$$N_\uparrow \propto \frac{1-P}{2}(I_+)_e + \frac{1+P}{2}(I_-)_e, \quad (\text{A2})$$

where we used $I_\pm = \frac{1}{2}\epsilon_0 cn|E_\pm|^2$ which is the intensity of the circular components. Finally, ΔT_\pm can be obtained by combining Eqs. (A2) and (6) and integrating the result over *y* (defined in the expression of y_e and y_r) to obtain the change in the total power of the right- and left-circularly polarized probe beam components.

$$\frac{\Delta T_{\pm}}{\Delta T_{\pm}|_{y=0}} = \frac{1+P^2}{2} G_w(y \pm d_r \mp d_e) + \frac{1-P^2}{2} G_w(y \pm d_r \pm d_e). \quad (\text{A3})$$

From Eq. (2) and the approximation $d^{(s,p)} \ll w_{e,r}$ in Eq. (A3) the measured SHEL displacement, \tilde{d} , is

$$\tilde{d}_{(PB)} = d_r - \rho_{(PB)} d_e, \quad (\text{A4})$$

where $\rho_{(PB)} = P^2$. From the definition of the degree of spin polarization, P , presented in Sec. II B 2, the derived expression for $\rho_{(PB)}$ as a function of measurable quantities such as the transmission change of a circularly probe beam induced by a circularly polarized pump beam is

$$\rho_{(PB)} = P^2 = \left| \frac{\Delta T_+ - \Delta T_-}{\Delta T_+ + \Delta T_-} \right|. \quad (\text{A5})$$

APPENDIX B: CALCULATIONS OF \tilde{d} OBTAINED VIA POLARIZATION DEPENDENT 2PA

Here, using the notation of the main body of the text, we provide a derivation for the measured SHEL displacement \tilde{d} using 2PA or the Kerr effect as the imaging mechanism for the SHEL.

We assume that the *excitation* (pump) beam and probe beam are both *p* or *s* polarized. We also consider a semiconductor with an index of refraction (typically $n \sim 3.6$ in our experiments) such that both beams propagate inside the material in a direction nearly antiparallel to the surface normal. While *s*-polarized light remains *s*-polarized (along *y*) in the medium, *p*-polarized light is nearly completely polarized along *x*, and we can therefore simplify subsequent calculations by neglecting the small component of the electric field along the *z* direction. The polarization of both beams is then in the *x*-*y* plane. Considering the SHEL acting on these beams, the linear polarization is split into its σ^{\pm} components separated by a polarization-dependent distance $d^{(s,p)}$ along the *y* direction given by Eq. (1). The polarization states of these beams inside the material are defined in Eq. (A1). Considering the approximation $d^{(s,p)} \ll w_{e(r)}$, we obtain for the polarization states of the beams inside the material,

$$\begin{aligned} \vec{E}_e &= E_e G_{w_e}(y_e) \hat{e} = \mathcal{E}_e \hat{e}, \\ \vec{E}_r &= E_r G_{w_r}(y_r) \hat{r} = \mathcal{E}_r \hat{r}, \end{aligned} \quad (\text{B1})$$

where

$$\hat{e}(\text{or } \hat{r}) = \frac{1}{\sqrt{2}}[(1 - \varepsilon_{e(r)})\sigma^+ + (1 + \varepsilon_{e(r)})\sigma^-] \quad (\text{B2})$$

and $\varepsilon_{e(r)}$ is the spatially varying degree of ellipticity of the beams,

$$\varepsilon_{e(r)} = \frac{y_{e(r)} d_{e(r)}}{w_{e(r)}^2}. \quad (\text{B3})$$

We calculate the polarization state of the probe beam inside the material using the wave equation in the slowly vary-

ing envelope approximation with a nonlinear polarization source term.³⁴ The positive frequency part of the optical field is governed by

$$\frac{\partial \vec{E}_a}{\partial z} = i \frac{\omega_s^2 \mu_0}{2k} \vec{P}_a^{NL} e^{-ik_a z} \quad (\text{B4})$$

where $\vec{P}_a^{NL} = \sum_{n=2}^{\infty} \vec{P}_a^{(n)}$. In the case of 2PA or the Kerr effect, we need to consider the third order nonlinear response corresponding to

$$\vec{P}_a^{NL}(\omega_a) = \varepsilon_0 K \vec{\chi}^{(3)}(-\omega_a; \omega_1, \omega_2, \omega_3) \cdot \vec{E}(\omega_1) \vec{E}(\omega_2) \vec{E}(\omega_3) e^{ik_a z}, \quad (\text{B5})$$

where $k_a = k_1 + k_2 + k_3$ and K is the numerical degeneracy coefficient. Since we focus on the pump-induced change to the σ^{\pm} components of the probe beam, we consider $(\vec{E}_{\pm})_r$ in Eq. (B4). This equation takes the form

$$\frac{\partial (\mathcal{E}_{\pm})_r}{\partial z} \sigma^{\pm} = \sigma^{\pm} i \frac{3k}{8} K \chi_{eff}(\sigma^{\pm}; \hat{e}^*, \hat{e}, \hat{r}) \mathcal{E}_e \mathcal{E}_e^* \mathcal{E}_r e^{i\Delta k z}, \quad (\text{B6})$$

with $\Delta k = 0$. We also use the concept of effective susceptibility to express the pump-induced 2PA/Kerr effect acting on the probe circular components³⁵

$$\begin{aligned} \chi_{eff}^{(3)}(\sigma^{\pm}; \hat{e}^*, \hat{e}, \hat{r}) &= [(\sigma^{\pm})^* \cdot \hat{e}^*](\hat{r}^* \cdot \hat{e}) \chi_{xyy} + \{[(\sigma^{\pm})^* \cdot \hat{e}](\hat{r} \cdot \hat{e}^*) \\ &\quad + [(\sigma^{\pm})^* \cdot \hat{r}]\} \chi_{xyy} + (\chi_{xxx} - \chi_{xyy} - 2\chi_{xyy}) \\ &\quad \times \sum_i (\sigma^{\pm})_i^* r_i |e_i|^2. \end{aligned} \quad (\text{B7})$$

The effective susceptibility carries a spatial dependence since the unit vectors \hat{e} and \hat{r} vary along the *y* direction. We then multiply Eq. (B6) by $(\mathcal{E}_{\pm} \sigma^{\pm})_r^*$ on both sides and solve for the intensity of the circular components of the probe assuming a regime of weak nonlinearity $\frac{k}{\varepsilon_0 c n^2} \chi_{eff} I_e L \ll 1$ as it is the case in our experiment. After the pump and probe beams have interacted over a distance *L* in the material, we obtain

$$I_{r\pm}(z) = I_r(0) \left(1 - \frac{3k}{2\varepsilon_0 c n^2} \chi_{eff}'' I_e (\mathcal{E}_{r\pm})_L \right) \quad (\text{B8})$$

where we used $I_{e(r)} = \frac{1}{2} \varepsilon_0 c n |E_{e(r)}|^2$ and the degeneracy factor $K = 2$.³⁵ This expression provides the total intensity of the circular components of the probe exiting the material for a given position along the *y* axis. The change in transmission of the circular components of the probe beam can be obtained by applying two operations on Eq. (B8). First, we drop terms not dependent on I_e since we are interested only in pump-induced changes to the probe beam. Then, we integrate Eq. (B8) in space (along *y* contained in the expressions for y_e and y_r) to obtain the total transmission of probe σ^+ and σ^- components.

For zincblende semiconductors with a (001) surface normal oriented so that the linear polarization of the incident beams is aligned along the [110], [011], [100], or [010] axis we find

$$\frac{\Delta T_{\pm}}{\Delta T_{\pm}|_{y=0}} = \left[\frac{y}{w_0^2} (1 \mp \eta_{(2PA)} d_r \mp \rho_{(2PA)} d_e) G_{w_0}(y) \right] \quad (\text{B9})$$

for the [110]- or [01̄1]-crystal axis contained within the plane of incidence

$$\begin{aligned} \eta_{(2PA)} &= \frac{(\chi''_{xxxx} + \chi''_{xyxy})}{(\chi''_{xxxx} + \chi''_{xxyy} + 2\chi''_{xyxy})}, \\ \rho_{(2PA)} &= \frac{(\chi''_{xyxy} - \chi''_{xxyy})}{(\chi''_{xxxx} + \chi''_{xxyy} + 2\chi''_{xyxy})}. \end{aligned} \quad (\text{B10})$$

However, if the [100]- or [010]-crystal axis is the one contained within the plane of incidence, we have

$$\begin{aligned} \eta_{(2PA)} &= \frac{(\chi''_{xxxx} + \chi''_{xyxy})}{2(\chi''_{xxxx})}, \\ \rho_{(2PA)} &= \frac{(\chi''_{xyxy} - \chi''_{xxyy})}{2(\chi''_{xxxx})}, \end{aligned} \quad (\text{B11})$$

From Eqs. (B9) and (2), \tilde{d} can be put in the same form as Eq. (5) using polarization dependent 2PA as the imaging mechanism for the SHEL,

$$\tilde{d}_{2PA} = \eta_{(2PA)} d_r - \rho_{(2PA)} d_e. \quad (\text{B12})$$

Note that both Eqs. (B10) and (B11) can also be expressed in terms of the effective susceptibilities such as

$$\begin{aligned} \eta_{(2PA)} &= \frac{\chi''_{eff}(\sigma^{\pm}; \hat{\ell}, \hat{\ell}, \sigma^{\pm})}{\chi''_{eff}(\hat{\ell}; \hat{\ell}, \hat{\ell}, \hat{\ell})}, \\ \rho_{(2PA)} &= \frac{\chi''_{eff}(\sigma^{\pm}; (\sigma^{\pm})^*, \sigma^{\pm}, \sigma^{\pm}) - \chi''_{eff}(\sigma^{\mp}; (\sigma^{\pm})^*, \sigma^{\pm}, \sigma^{\mp})}{2\chi''_{eff}(\hat{\ell}; \hat{\ell}, \hat{\ell}, \hat{\ell})} \end{aligned} \quad (\text{B13})$$

where $\hat{\ell}$ is a linear polarization state, for both incident pump and probe beams in the SHEL experiment, which, in the most general case, can be oriented along the [110]-, [01̄1]-, [100]- or [010]-crystal axis.

As mentioned previously, Eq. (B13) can be used to determine experimentally the value of $\eta_{(2PA)}$ and $\rho_{(2PA)}$ since the pump-probe 2PA coefficient (β) is proportional to $\chi''_{eff}[\hat{r}; (\hat{\ell})^*, \hat{e}, \hat{r}]$.

*jmenard@physics.utoronto.ca

[†]Present address: Experimentelle Physik 2, Technische Universität Dortmund, 44221 Dortmund, Germany.

¹F. I. Fedorov, Dokl. Akad. Nauk SSSR **105**, 465 (1955).

²C. Imbert, Phys. Rev. D **5**, 787 (1972).

³M. Onoda, S. Murakami, and N. Nagaosa, Phys. Rev. Lett. **93**, 083901 (2004).

⁴K. Y. Bliokh and Y. P. Bliokh, Phys. Rev. Lett. **96**, 073903 (2006).

⁵K. Y. Bliokh and Y. P. Bliokh, Phys. Rev. E **75**, 066609 (2007).

⁶O. Hosten and P. Kwiat, Science **319**, 787 (2008).

⁷A. Aiello and J. P. Woerdman, Opt. Lett. **33**, 1437 (2008).

⁸C. Menzel, C. Rockstuhl, T. Paul, S. Fahr, and F. Lederer, Phys. Rev. A **77**, 013810 (2008).

⁹K. Y. Bliokh, I. V. Shadrivov, and Y. S. Kivshar, Opt. Lett. **34**, 389 (2009).

¹⁰D. Haefner, S. Sukhov, and A. Dogariu, Phys. Rev. Lett. **102**, 123903 (2009).

¹¹A. Aiello, M. Merano, and J. P. Woerdman, Opt. Lett. **34**, 1207 (2009).

¹²Y. Qin, Y. Li, H. He, and Q. Gong, Opt. Lett. **34**, 2551 (2009).

¹³C.-F. Li, Phys. Rev. A **80**, 063814 (2009).

¹⁴H. Luo, S. Wen, W. Shu, Z. Tang, Y. Zou, and D. Fan, Phys. Rev. A **80**, 043810 (2009).

¹⁵J.-M. Ménard, A. E. Mattacchione, M. Betz, and H. M. van Driel, Opt. Lett. **34**, 2312 (2009).

¹⁶Y. K. Kato, R. C. Myers, A. C. Gossard, and D. D. Awschalom, Science **306**, 1910 (2004).

¹⁷O. C. de Beauregard, C. Imbert, and Y. Levy, Phys. Rev. D **15**,

3553 (1977).

¹⁸L. Dutriaux, A. L. Floch, and F. Bretenaker, EPL **24**, 345 (1993).

¹⁹F. Pillon, H. Gilles, and S. Girard, Appl. Opt. **43**, 1863 (2004).

²⁰J. J. Cowan and B. Anicin, J. Opt. Soc. Am. **67**, 1307 (1977).

²¹V. G. Fedoseyev, J. Phys. A **21**, 2045 (1988).

²²M. A. Player, J. Phys. A **20**, 3667 (1987).

²³H. Schilling, Ann. Phys. **471**, 122 (1965).

²⁴J. Ricard, Nouv. Rev. Opt. **5**, 7 (1974).

²⁵V. S. Liberman and B. Y. Zel'dovich, Phys. Rev. A **46**, 5199 (1992).

²⁶B.-Y. Liu and C.-F. Li, Opt. Commun. **281**, 3427 (2008).

²⁷A. Aiello, M. Merano, and J. P. Woerdman, Phys. Rev. A **80**, 061801(R) (2009).

²⁸F. Meier and B. P. Zakharchenya, *Optical Orientation* (North-Holland, Amsterdam, 1984).

²⁹D. J. Hilton and C. L. Tang, Phys. Rev. Lett. **89**, 146601 (2002).

³⁰B. R. Bennett, R. A. Soref, and J. Del Alamo, IEEE J. Quantum Electron. **26**, 113 (1990).

³¹P. Langot, R. Tommasi, and F. Vallée, Phys. Rev. B **54**, 1775 (1996).

³²V. Grivickas, J. Linnros, A. Vigelis, J. Seckus, and J. A. Tellefson, Solid-State Electron. **35**, 299 (1992).

³³R. W. Schoenlein, W. Z. Lin, S. D. Brorson, E. P. Ippen, and J. G. Fujimoto, Solid-State Electron. **31**, 443 (1988).

³⁴P. N. Butcher and D. Cotter, *The Elements of Nonlinear Optics* (Cambridge University Press, New York, NY, 1991).

³⁵D. C. Hutchings and B. S. Wherrett, Phys. Rev. B **52**, 8150 (1995).